A HYBRID NEURAL NETWORK MODEL FOR THE DYNAMICS OF THE KURAMOTO-SIVASHINSKY EQUATION

NEJIB SMAOUI

Received 2 January 2004 and in revised form 14 February 2004

A hybrid approach consisting of two neural networks is used to model the oscillatory dynamical behavior of the Kuramoto-Sivashinsky (KS) equation at a bifurcation parameter $\alpha = 84.25$. This oscillatory behavior results from a fixed point that occurs at $\alpha = 72$ having a shape of two-humped curve that becomes unstable and undergoes a Hopf bifurcation at $\alpha = 83.75$. First, Karhunen-Loève (KL) decomposition was used to extract five coherent structures of the oscillatory behavior capturing almost 100% of the energy. Based on the five coherent structures, a system of five ordinary differential equations (ODEs) whose dynamics is similar to the original dynamics of the KS equation was derived via KL Galerkin projection. Then, an autoassociative neural network was utilized on the amplitudes of the ODEs system with the task of reducing the dimension of the dynamical behavior to its intrinsic dimension, and a feedforward neural network was used to model the dynamics at a future time. We show that by combining KL decomposition and neural networks, a reduced dynamical model of the KS equation is obtained.

1. Introduction

During the last two decades, similarities between the theories of ordinary differential equations (ODEs) and partial differential equations (PDEs) have been observed in the context of the qualitative theory of differential equations, especially in the case of parabolic PDEs. In 1981, Henry [13] gave various examples of this trend, comparing the stability properties of PDEs to those of ODEs. Later on, the work of Mallet-Paret [24], Mañé [25], and others opened up new avenues for understanding the longtime dynamics of a more general class of dissipative PDEs. Furthermore, the results of Babin and Vishik, Constantin et al., Foias et al., and Ladyzhenskaya [3, 7, 8, 9, 10, 21], who proved the finite dimensionality of the global attractor of the two-dimensional (2D) Navier-Stokes (NS) equations, strengthened the similarities between the two fields. The results suggest that the dynamics on the attractor can be captured by a system of ODEs making the longtime dynamics of the PDEs equivalent in some sense to the dynamics of a suitable system

Mathematical Problems in Engineering 2004:3 (2004) 305–321
2000 Mathematics Subject Classification: 35K55, 37N10, 37E99
URL: http://dx.doi.org/10.1155/S1024123X0440101X

of ODEs. In 1997, a system of ODEs that mimics the dynamics of the 2D NS flow for a given Reynolds number has been constructed by Smaoui and Armbruster [34]. Similar to the 2D NS equations, the one-dimensional (1D) Kuramoto-Sivashinsky (KS) equation was proven to contain a finite-dimensional global attractor [1]. Kirby and Armbruster [18] and Smaoui and Zribi [35] have each obtained a system of ODEs for the 1D KS equation based on Karhunen-Loève (KL) Galerkin approach for a given bifurcation parameter $\alpha = 17.75$. In [35], three different finite-dimensional feedback control schemes of the KS equation were designed for the system of ODEs with the task of stabilizing its dynamics.

Recently, Neural networks have been used for the prediction of complicated dynamics and the identification of long-term dynamical behavior and bifurcation [5, 11, 27, 29, 30]. Neural networks in conjunction with KL decomposition were also used to model the unstable manifold of the bursting behavior in the 2D NS equations [31], to unravel the complex behavior observed in 2D flames [33] and to obtain the intrinsic dimension of the dynamics of the 2D NS equations and the 1D KS equation [32]. The greatest advantage of a neural network is its ability to model complex nonlinear relationships without any assumptions about the nature of the relationships.

The goal of this paper is to obtain a reduced dynamical system for the 1D KS equation based on a hybrid approach that combines KL decomposition and artificial neural networks. We extend the ideas presented in [32] to demonstrate that this new modelling approach can be used to elucidate the dynamics of more complicated PDEs, such as the NS equation and related problems.

The paper is organized as follow. In Section 2, we present some numerical simulation results of the KS equation for a bifurcation parameter $\alpha = 84.25$. In Section 3, we apply the KL decomposition to the numerical simulation results and show that the dynamics of the KS equation studied in Section 1 can be represented in phase space by a limit cycle. Furthermore, a system of five ODEs based on a KL Galerkin approach is then obtained and it reduces the KS equation faithfully to a model with a minimum degree of freedom. Section 4 presents a hybrid neural network model consisting of an autoassociative neural network and a feedforward neural network, with phase space dimension equal to the intrinsic dimension of the KS equation, and some concluding remarks are given in Section 5.

2. The Kuramoto-Sivashinsky equation

In the last two decades, many theoretical and numerical studies were devoted to the KS equation [1, 15, 17, 18, 20, 32, 35]. The KS equation

$$\frac{\partial u}{\partial t} + \nu \frac{\partial^4 u}{\partial x^4} + \frac{\partial^2 u}{\partial x^2} + \frac{1}{2}\left(\frac{\partial u}{\partial x}\right)^2 = 0, \quad (x,t) \in \mathbb{R}^1 \times \mathbb{R}^+, \tag{2.1}$$

$$u(x,t) = u(x+L,t), \tag{2.2}$$

$$u(x,0) = u_0(x), \tag{2.3}$$

where L is a period and ν is the kinematic viscosity, can be transformed to the following equation:

$$\frac{\partial u}{\partial t}+4\frac{\partial^4 u}{\partial x^4}+\alpha\left[\frac{\partial^2 u}{\partial x^2}+\frac{1}{2}\left(\frac{\partial u}{\partial x}\right)^2\right]=0,\quad 0\le x\le 2\pi, \tag{2.4}$$

$$u(x,t)=u(x+2\pi,t), \tag{2.5}$$

$$u(x,0)=u_0(x), \tag{2.6}$$

by setting $\tilde{t}=\nu t/4$, $L=2\pi$, and introducing a new bifurcation parameter $\alpha=4/\nu$. The mean value of u is given by

$$m(t)=\frac{1}{2\pi}\int_0^{2\pi}u(x,t)dx, \tag{2.7}$$

and the rate of change of m with respect to time satisfies the drift equation

$$\dot{m}(t)=\frac{-\alpha}{4\pi}\int_0^{2\pi}(u_x)^2dx. \tag{2.8}$$

To normalize the drift to zero, we modify (2.4) by setting

$$v(x,t)=u(x,t)-m(t). \tag{2.9}$$

The drift-free KS equation becomes

$$\frac{\partial v}{\partial t}+4\frac{\partial^4 v}{\partial x^4}+\alpha\left[\frac{\partial^2 v}{\partial x^2}+\frac{1}{2}\left(\frac{\partial v}{\partial x}\right)^2\right]+\dot{m}(t)=0,\quad 0\le x\le 2\pi, \tag{2.10}$$

$$v(x,t)=v(x+2\pi,t), \tag{2.11}$$

$$v(x,0)=v_0(x). \tag{2.12}$$

In [15], it has been shown that as α increases from 0 to 320, the dynamics exhibits a variety of interesting behaviors including fixed points, traveling waves, beating waves, homoclinic and heteroclinic orbits, and chaos. For the bifurcation parameter $\alpha=84.25$, the dynamics of the KS equation is shown to exhibit a local oscillatory motion [15, 18]. In [18], it was explained that this behavior resulted from a Hopf bifurcation of a "strange" fixed point that becomes unstable at $\alpha=83.75$.

Since the goal of this work is to obtain a reduced dynamical system for the KS equation at $\alpha=84.25$, we numerically compute the time series solution of (2.10), (2.11), and (2.12) with $v_0(x)=\sin 2x+\sin 3x+\cos x+\cos 4x$ by decomposing $v(x,t)$ via the expansion

$$v(x,t)=\sum_{k=-\infty}^{\infty}a_k(t)e^{ikx}. \tag{2.13}$$

Using the above expansion, (2.10) becomes

$$\sum_{k=-\infty}^{\infty}\left[\dot{a}_k(t)+\left(4k^4-\alpha k^2\right)a_k(t)\right]e^{ikx}=\frac{\alpha}{2}\left(\sum_{k=-\infty}^{\infty}ka_k(t)e^{ikx}\right)^2-\dot{m}(t). \tag{2.14}$$

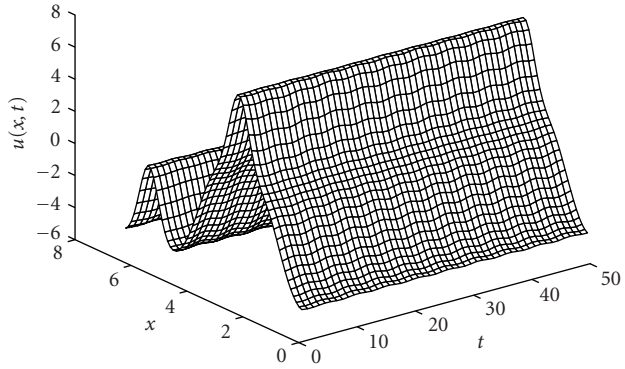

Figure 2.1. Numerical simulation results of the KS equation at $\alpha = 84.25$ with initial conditions $v_0(x) = \sin 2x + \sin 3x + \cos x + \cos 4x$.

The Fourier coefficients a_k are found via the orthogonality relationship

$$\int_0^{2\pi} e^{ikx} e^{-ilx} dx = 2\pi\delta_{kl}. \tag{2.15}$$

Carrying out this procedure and truncating the expansion results in

$$\dot{a}_l(t) = (\alpha l^2 - 4l^4) a_l(t) + \frac{\alpha}{2} \sum_{n=-N+l}^{N} n(l-n) a_{l-n} a_n, \tag{2.16}$$

where $-N \le l \le N$. Equation (2.16) is solved using a pseudospectral Galerkin method [6].

Figure 2.1 presents a numerical simulation result obtained at $\alpha = 84.25$. Looking carefully at Figure 2.1, we see that it consists of a local oscillatory behavior. For $\alpha = 72$, the PDE has an attracting fixed point. This fixed point has a shape of a two-humped curve, one hump smaller than the other, and it is known as "strange fixed point." At $\alpha = 83.75$, this fixed point becomes unstable and undergoes a Hopf bifurcation which results in the oscillatory behavior shown in Figure 2.1. In the phase space concept, the behavior is similar to that of a limit cycle. To extract the coherent structure of the dynamics shown in Figure 2.1, we decompose the numerical simulation results using KLTOOL (see [2]). To make this paper self-contained, we briefly describe the KL decomposition.

3. The Karhunen-Loève decomposition

The KL decomposition is a method of representing a set of data with a minimum degree of freedom. In the literature, KL decomposition goes under a variety of other names such as Hotelling transform [14], principle component analysis [16], factor analysis [12], empirical orthogonal functions [22], and singular value decomposition (SVD) or proper orthogonal decomposition (POD) [23]. KL decomposition produces a basis of orthogonal functions, ψ_n, that span the data in an optimal way. The basis is optimal in the sense that a truncated series representation of the data in this basis has a smaller mean square error than that of a representation of the data by any other basis. As a means of

explaining the KL decomposition, we select a set of real (random) vectors, which depend on space and time, $\{v_i\}_{i=1}^{M}$. This set of vectors is called "snapshots" [28]. It was shown that the most coherent structures, $\psi(x)$, among these snapshots are given by solving the eigenvalue problem of the integral equation given by

$$\int K(x,x')\psi(x')dx' = \lambda\psi(x), \tag{3.1}$$

where the kernel defined by

$$K(x,x') = \lim_{M\to\infty} \frac{1}{M}\sum_{i=1}^{M} v_i(x)v_i^T(x') \tag{3.2}$$

can be approximated by

$$K(x,x') \approx \frac{1}{M}\sum_{i=1}^{M} v_i(x)v_i^T(x') \tag{3.3}$$

for a sufficiently large M [28, 32, 35].

Expanding the snapshots v_i in terms of these eigenfunctions, we get

$$v_i = v(x,t_i) = \sum_{k=1}^{M} a_k(t_i)\psi_k(x), \tag{3.4}$$

where $\psi_k(x)$ are the time-independent eigenfunctions that show the important structures, and $a_k(t_i)$ are the time-dependent amplitudes that show how the structure in time interacts and may be found by projecting the snapshots v_i onto an eigenfunction:

$$a_k(t_i) = \frac{(v_i,\psi_k)}{(\psi_k,\psi_k)}. \tag{3.5}$$

To each eigenfunction an energy percentage is assigned based on the eigenfunction's associated eigenvalue, that is, $E_k = \lambda_k/E$. The eigenfunction ψ_1 corresponding to the largest energy is the most coherent structure of the snapshots $\{v_i\}_{i=1}^{M}$, and the eigenfunction ψ_2 with the next largest energy is the next coherent structure, and so forth.

Using only the first most energetic N eigenfunctions, an approximation of the data is constructed:

$$v(x,t_i) \approx \sum_{k=1}^{N} a_k(t_i)\psi_k(x). \tag{3.6}$$

The KL procedure has been used on the numerical results obtained in Figure 2.1 with the task of extracting the coherent structures or the most energetic eigenfunctions of the numerical data. Figure 3.1 depicts the five most energetic eigenfunctions accounting for 99.99% of the total energy. The first eigenfunction corresponds to the fixed point attractor that occurs at $\alpha = 72$ which becomes unstable. The remaining four eigenfunctions describe the local oscillation. This suggests that the dynamical behavior presented by the

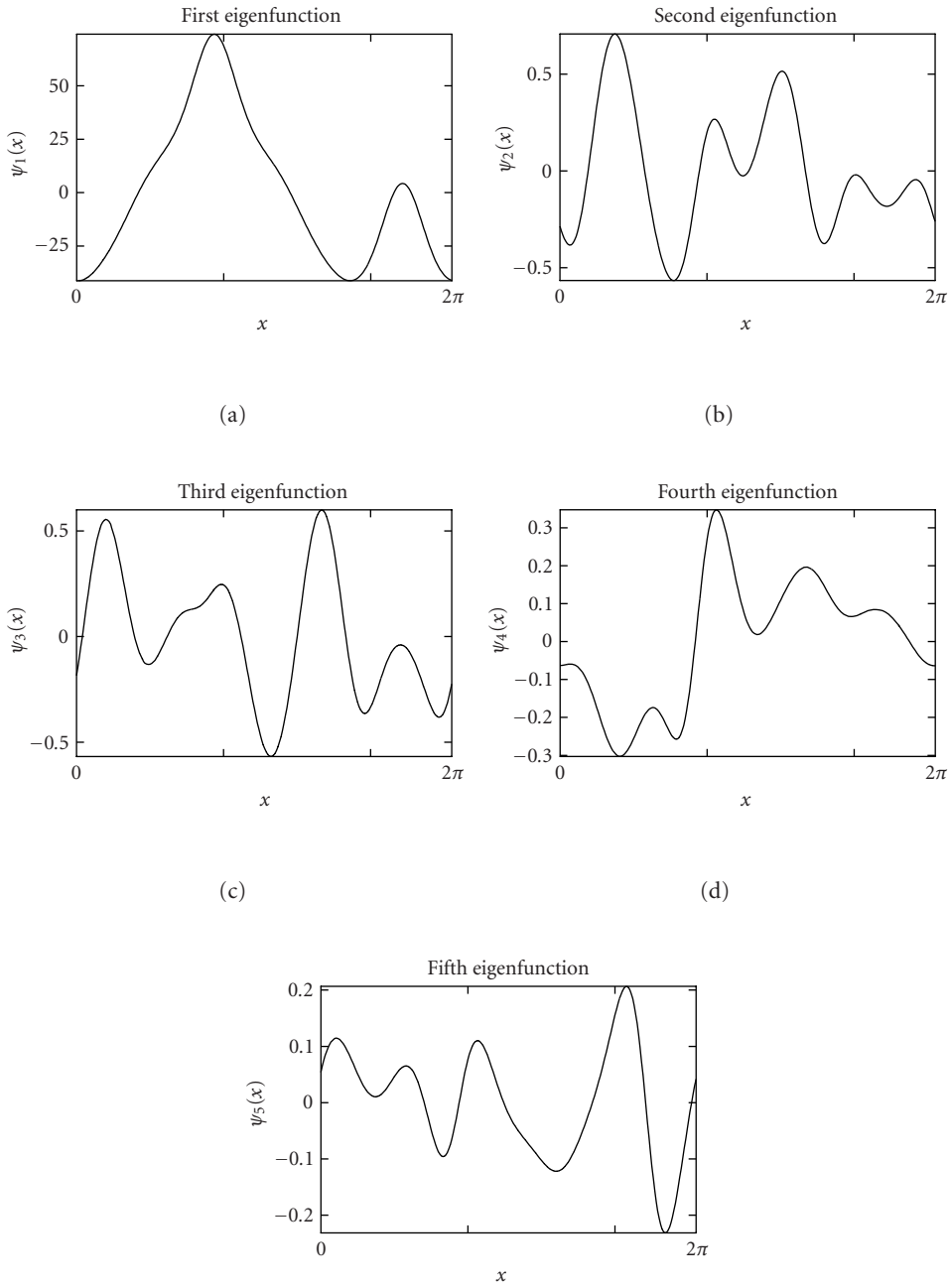

Figure 3.1. The first five eigenfunctions of the KS numerical simulation data at $\alpha = 84.25$.

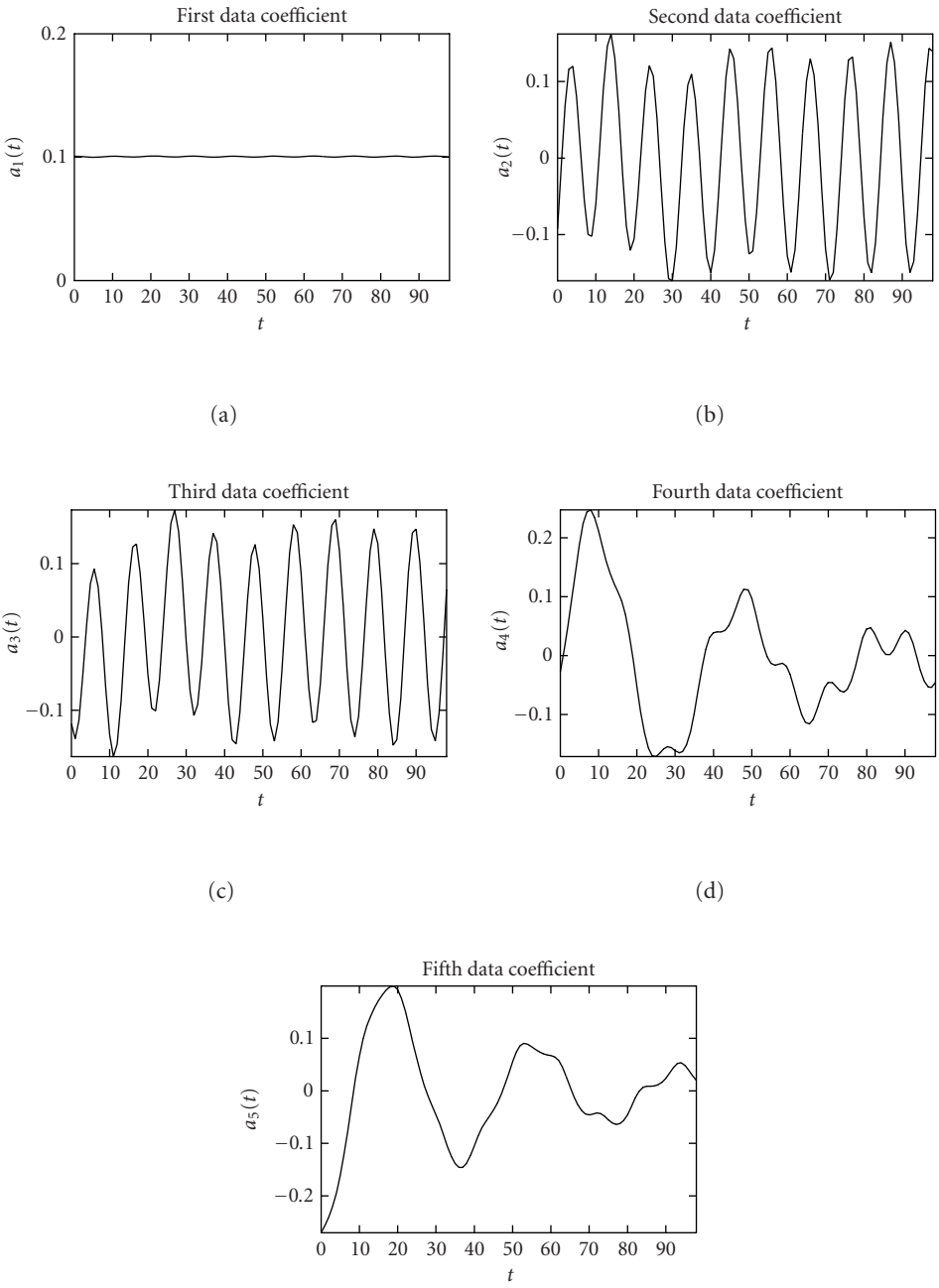

Figure 3.2. The first five data coefficients of the numerical simulation data shown on Figure 2.1.

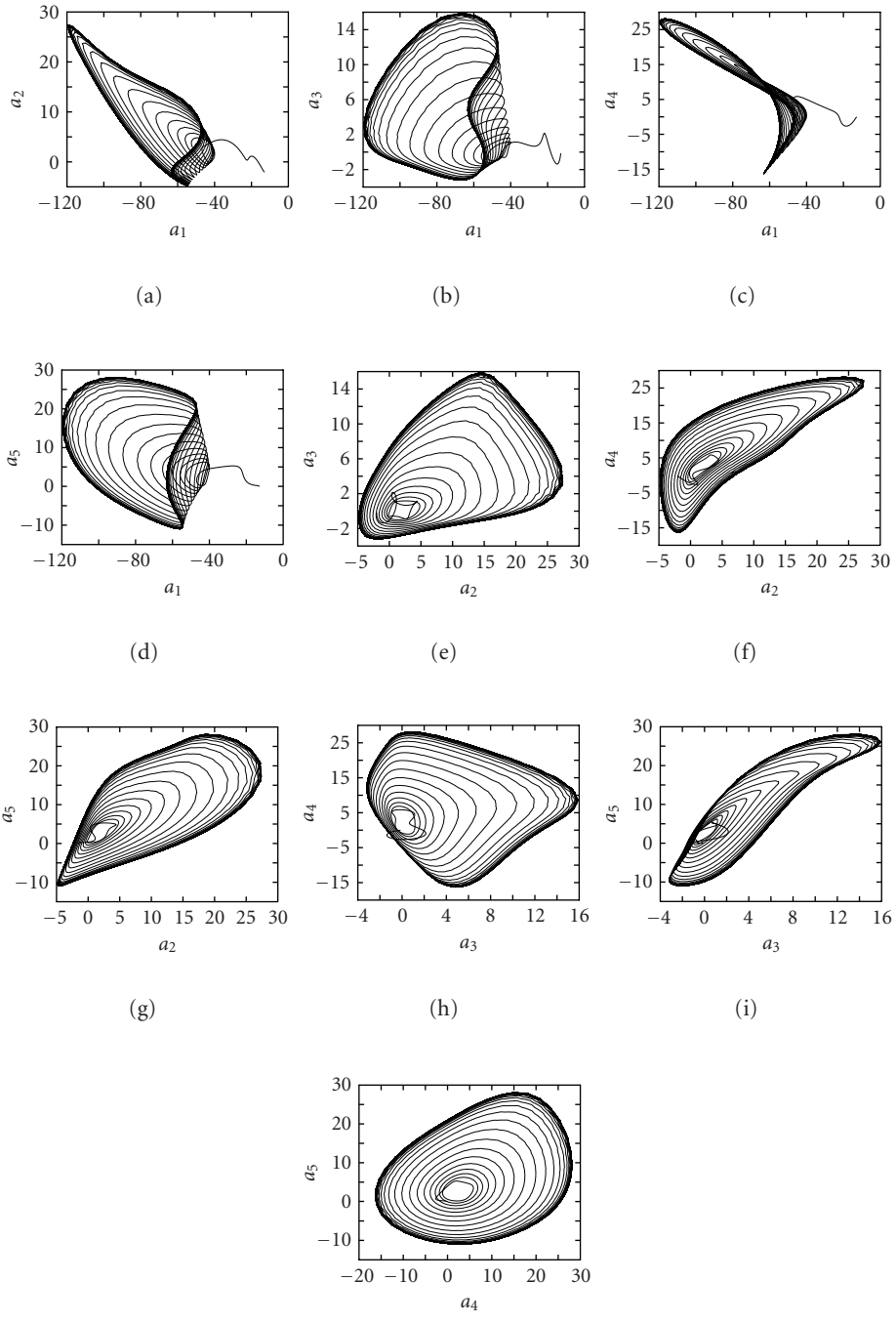

Figure 3.3. Different projections of the limit cycle from a five-dimensional phase space into two dimensions.

local oscillatory behavior lives in a low-dimensional linear space, and that the KL expansion provides a set of vectors that span this space. Of course, the dimension of this space is not the intrinsic dimension where the attractor resides, since in phase space the periodic solution is presented by a limit cycle which may be viewed topologically as a one-dimensional manifold (see Smaoui [32]). Projections of the numerical results onto the first five eigenfunctions are given in Figure 3.2.

The derivation of the system of ODEs based on KL eigenfunctions is similar to the Fourier-Galerkin projection presented above. The new decomposition takes the form

$$v(x,t) \approx \sum_{k=1}^{N} a_k \psi_k, \tag{3.7}$$

where

$$\psi_k = \sum_{l=-H}^{H} c_{lk} e^{ilx}. \tag{3.8}$$

Thus,

$$\dot{a}_m(t) = -4 \sum_{n=1}^{\infty} a_n(\psi_m, \psi_n^{(4)}) - \alpha \sum_{n=1}^{\infty} a_n(\psi_m, \psi_n'') - \frac{\alpha}{2} \sum_{n,k=1}^{\infty} (\psi_m, \psi_k' \psi_n') a_n a_k. \tag{3.9}$$

Equation (3.9) was obtained by substituting $v(x,t)$ from (3.7) into (2.10), multiplying by ψ_m, $m = 1,\ldots,N$, integrating from 0 to 2π, and applying the orthogonality condition of the $\psi_k's$.

Truncating the expansion of $v(x,t)$ in terms of the KL eigenfunctions to $N = 5$ (i.e., considering only the first five most energetic eigenfunctions) results in a system of five ODEs (see the appendix). The cubic damping term in each equation was artificially added to mimic dissipation carried out by the smaller scales as suggested by Kirby and Armbruster [18]. After numerically integrating the system of ODEs and plotting the time series solutions versus one another, a limit cycle appears in a five-dimensional space projected in two dimensions (see Figure 3.3). Since the topological dimension of this limit cycle is one, then we use the theory presented in [19, 32] to obtain a dynamical model with attractor's dimension equal to one. This dynamical model based on neural networks is presented in the following section.

4. The hybrid neural network model

Our hybrid neural network modelling approach consists of designing two neural networks in series, where the first is an autoassociative neural network designed to reduce the dimensionality of the problem to its intrinsic dimension, and the second is a feedforward neural network used for prediction. We now describe the two neural networks.

4.1. The autoassociative neural network. An autoassociative neural network is a network capable of reducing the dimensionality of the data with minimum information loss (see Figure 4.1). Figure 4.1 consists of five layers: a five-node input layer, two ten-node

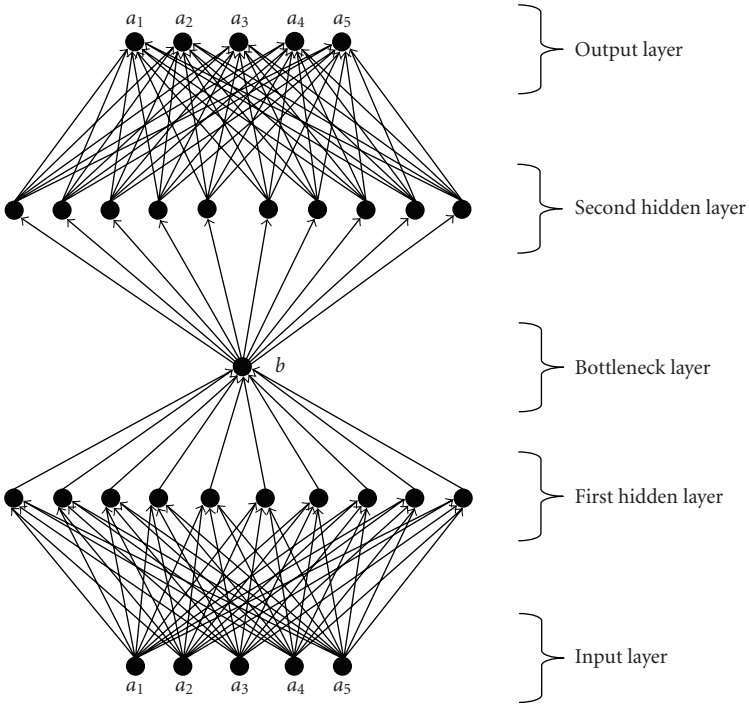

Figure 4.1. The autoassociative neural network used for dimensionality reduction.

hidden layers with nonlinear sigmoidal activation function $g(x) = \tanh x$, one-node bottleneck layer, and a five-node output layer that consists of the same values of the input layer nodes. Baldi and Hornik [4] have shown that if only one bottleneck layer is used between the input and the output layers, then the network extracts the principal components or the coherent structures of the data as defined earlier in Section 3. KL decomposition projects the data into a linear subspace with a minimum information loss. This linear subspace is obtained by multiplying the data by the eigenvectors of the covariance matrix defined in (3.3), thus extracting a set of eigenfunctions or coherent structures that span the linear subspace in an optimal way. By examining the energy of the corresponding eigenfunctions, one can estimate the minimum dimensionality of the space into which the data can be projected and thus eliminate the loss. However, if the data lie on a nonlinear submanifold of the feature space, then KL decomposition will overestimate the phase space dimension of the data. For example, the dynamics of the KS equation at $\alpha = 84.25$ represented in phase space by a limit cycle was captured using five eigenfunctions. However, the limit cycle is a one-dimensional manifold and can be smoothly parameterized with a single number.

To provide a network capable of extracting nonlinear features, one hidden layer is added between the input layer and the bottleneck layer and another one between the bottleneck layer and the output layer with nonlinear sigmoidal activation function (see

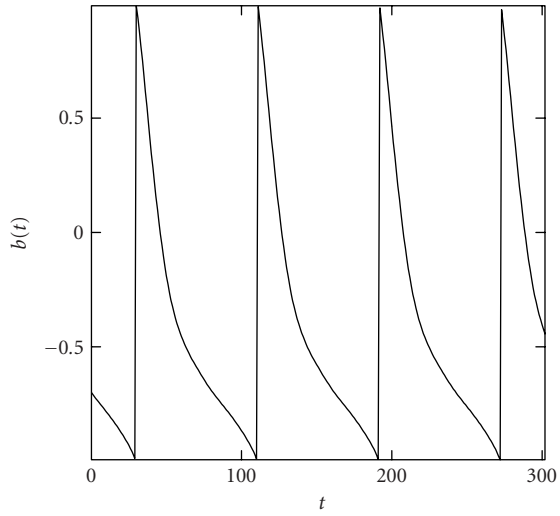

Figure 4.2. The time evolution of $b(t)$ at the bottleneck node.

Kramer [19] and Smaoui [32]). Such a network can perform the nonlinear analogue of KL decomposition and extract nonlinear principal manifolds.

The number of nodes in the input layer consists of the amplitudes $\{a_i\}_{i=1}^{5}$ derived from (3.9), which represent solutions of the system of differential equations at different times. The number of nodes in the output layer is the same as the number of nodes in the input layer. That is, the network presented in Figure 4.1 is trained to reproduce the identity mapping

$$I_d : \mathbb{R}^n \xrightarrow{F} \mathbb{R}^p \xrightarrow{F^{-1}} \mathbb{R}^n, \tag{4.1}$$

where $p < n$. In general, in order to find the value of p, the network should be pruned in the same way as in [32, 33]. In our case, there is no need to prune the network since p is equal to 1 which is the attractor intrinsic dimension of the KS dynamics at $\alpha = 84.25$. Three hundred sets of data, where each set constitutes the amplitudes $\{a_i\}_{i=1}^{5}$, were used during the training process. Upon convergence of the network, the values of the node at the bottleneck layer are saved. Figure 4.2 depicts the evolution of the values of the bottleneck node as a function of time. This procedure reduces the phase space of the dynamical behavior from a five-dimensional space into a one-dimensional one. Next, the feedforward neural network presented in Figure 4.3 is used to model the dynamics of $b(t)$ for future prediction.

4.2. The feedforward neural network. Feedforward neural networks have been used for the prediction of complicated dynamics and the identification of long-term dynamical behavior and bifurcation [5, 11, 27, 29, 30, 31]. In this subsection, we design a feedforward neural network to obtain a nonlinear input-output map, which, given the values of $b(t)$ at times t_n and t_{n-1}, will predict the value of $b(t)$ at time t_{n+P} for different values of P

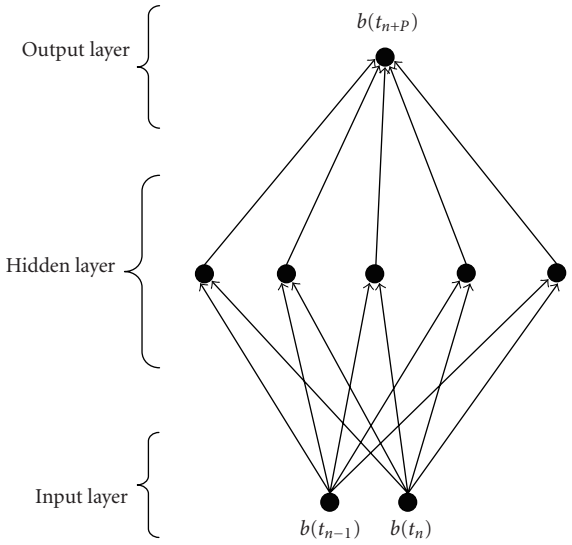

Figure 4.3. The feedforward neural network used for future prediction.

(see Figure 4.3). The network consists of three layers: a two-node input layer, a five-node hidden layer, and a one-node output layer. The input to each node is a weighted sum of outputs of the nodes in the previous layer. Each hidden layer node performs a nonlinear transformation of its input:

$$O_i = g\left(\sum_j w_{ij}x_j - \theta_i\right), \tag{4.2}$$

where O_i is the node output, x_j is the node input (outputs of the previous layers), w_{ij} are the weights, and θ_i is a bias (w_{ij} and θ_i are adjustable parameters of the model). The transfer function $g(x) = \tanh x$ is a sigmoidal function that takes the input (which may have any value between plus and minus infinity) and squashes the output into the range from -1 to 1.

The node in the output layer predicts the value of $b(t)$ at the next P sampling instant $b(t_{n+P})$, that is, we have the following mapping:

$$b(t_{n+P}) = f(b(t_n), b(t_{n-1})), \tag{4.3}$$

where f is a set of nonlinear functions representing the neural network model.

During the training procedure, the network compares its actual response with the target response and adjusts its weights in such a way to minimize the sum square of the error E defined by

$$E = \frac{1}{2}\sum_p \sum_k (z_k - y_k)_p^2, \tag{4.4}$$

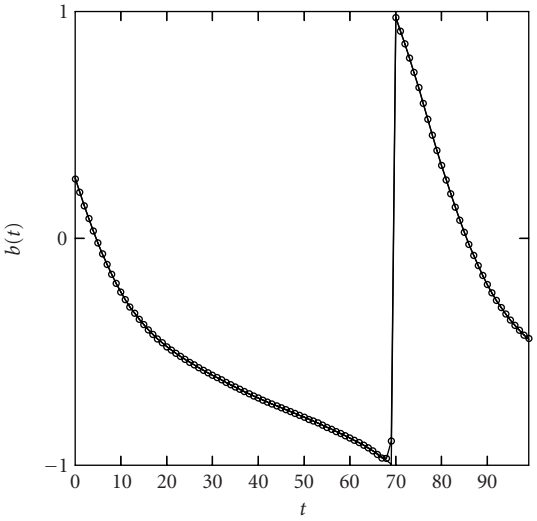

Figure 4.4. Short-term neural network prediction of $b(t)$ (solid) versus its original values (circles).

where z_k is the desired vector of the kth output node, y_k is the actual output vector of the kth output node, and the subscript p refers to the specific input vector pattern used. The weights are successfully modified in order to reduce E. The Levenberg-Marquardt algorithm which has proven to be a reliable and efficient algorithm for computing the weight matrix was used [26].

For $P = 1$ in (4.3), a sensitivity study was conducted to fine-tune both the sum square error and the number of nodes in the hidden layer. The network was then trained using the first 200 sets of the data given in Figure 4.2, where each set contains the values of $b(t)$ at times t_n and t_{n-1}. Upon convergence, that is, when the sum square error reaches a preset bound, the weights connecting all nodes were saved and the network was tested for the remaining sets of data not included during the training stage (i.e., the last 100 data sets in Figure 4.2). Figure 4.4 presents both the testing data sets and their neural network predictions. The almost perfect match of the predicted coefficients of $b(t)$ with the original ones indicates the ability of the hybrid model to capture the dynamical behavior of the KS equation at $\alpha = 84.25$. The model

$$b(t_{n+1}) = f(b(t_n), b(t_{n-1})) \tag{4.5}$$

can be represented in terms of the saved weights and biases:

$$b(t_{n+1}) = \mathbf{w}^{(2)} g(\mathbf{w}^{(1)} \mathbf{b}(t_n, t_{n-1}) - \boldsymbol{\theta}_1) - \boldsymbol{\theta}_2, \tag{4.6}$$

where $\mathbf{w}^{(1)}$ is the weight matrix for synapses connecting the input nodes with nodes of the first hidden layer, and $\mathbf{w}^{(2)}$ is the weight matrix for synapses connecting the first hidden

layer with the node at the output layer. These weights are given by

$$\mathbf{w}^{(1)} = \begin{bmatrix} -86.1253 & -55.4127 \\ 1.535 & -2.3512 \\ 0.0076 & 0.2551 \\ -8.1596 & -81.7548 \\ -67.8001 & -32.0746 \end{bmatrix}, \tag{4.7}$$

$$\mathbf{w}^{(2)} = \begin{bmatrix} -1.8116 & -0.7044 & 8.2458 & -43.8703 & 42.9676 \end{bmatrix}.$$

The bias vectors used for each layer $\boldsymbol{\theta}_1$ and $\boldsymbol{\theta}_2$ are given by

$$\boldsymbol{\theta}_1 = \begin{bmatrix} -137.633 \\ -0.8655 \\ -1.2115 \\ -89.5293 \\ -98.2105 \end{bmatrix}, \qquad \boldsymbol{\theta}_2 = [3.6765]. \tag{4.8}$$

$\mathbf{b}(t_n, t_{n-1}) = \begin{pmatrix} b(t_n) \\ b(t_{n-1}) \end{pmatrix}$ and $b(t_{n+1})$ are the input and output vectors that consist of the values of the data coefficients at t_{n-1}, t_n and t_{n+1}, respectively.

The architecture given in Figure 4.3 was also used to predict the values at the bottleneck node when $P = 3, 6$, and 9. Excellent agreement was found in each case. It should be noted that a prediction at P time steps into the future past the last observed point $b(t)$ will be made using observed data at times: $b(t)$ and $b(t-1)$. That is, a prediction at P time steps into the future is made by placing previously predicted values in the input layer. For large enough P, good predictions might not be achieved. Of course, this can happen because previously predicted values (made with some errors) are used to make a subsequent prediction; therefore the errors get magnified upon iterations.

5. Concluding remarks

A hybrid approach consisting of two neural networks was used to model the dynamics of the KS equation. Numerical solutions using pseudospectral techniques were obtained at a bifurcation parameter $\alpha = 84.25$. Coherent structures were extracted from the numerical simulation results via KL decomposition. Then, a system of five ODEs was derived using KL Galerkin projection whose dynamical behavior is similar to the KS equation and is represented by a limit cycle in a five-dimensional space. An autoassociative neural network utilized for dimensionality reduction and a feedforward network used for prediction were combined in series to model the dynamics of the KS equation at a future time. The model was successful in predicting the dynamics at different time steps.

It should be emphasized that the hybrid approach presented is not limited only to the dynamics of PDEs, but it can also be carried out to model the dynamical behavior of experimental data. In such a case, KL data coefficients will be used as inputs to the autoassociative neural networks instead of the amplitudes of the ODEs system.

Appendix

The system of ODEs

The following system of ODEs was derived by applying the KL Galerkin projection to the five most energetic eigenfunctions of the KS equation at $\alpha = 84.25$:

$$
\begin{aligned}
\dot{a}_1 &= -101.795a_1 + 2.76107\alpha a_1 - 0.64364\alpha a_1^2 - 26.1487a_2 + 0.418203\alpha a_2 \\
&\quad + 1.27714\alpha a_1 a_2 - 0.7451\alpha a_2^2 - 72.8953a_3 + 0.725986\alpha a_3 - 1.41632\alpha a_1 a_3 \\
&\quad - 3.50667\alpha a_2 a_3 + 4.26641\alpha a_3^2 - 12.4719a_4 + 0.375998\alpha a_4 - 0.940871\alpha a_1 a_4 \\
&\quad - 10.7512\alpha a_2 a_4 - 1.05421\alpha a_3 a_4 - 6.43332\alpha a_4^2 + 34.6688a_5 - 0.561543\alpha a_5 \\
&\quad - 0.218701\alpha a_1 a_5 - 8.07564\alpha a_2 a_5 - 2.1708\alpha a_3 a_5 - 9.58715\alpha a_4 a_5 + 0.161873\alpha a_5^2 \\
&\quad - 1.5a_1^3, \\
\dot{a}_2 &= -26.1487a_1 + 0.418203\alpha a_1 - 0.0461221\alpha a_1^2 - 1037.64a_2 + 13.0649\alpha a_2 \\
&\quad + 0.121569\alpha a_1 a_2 - 1.54634\alpha a_2^2 + 122.542a_3 - 1.00856\alpha a_3 + 4.06744\alpha a_1 a_3 \\
&\quad + 1.12682\alpha a_2 a_3 - 1.54545\alpha a_3^2 - 201.511a_4 + 1.49775\alpha a_4 + 1.38514\alpha a_1 a_4 \\
&\quad + 3.55207\alpha a_2 a_4 - 2.48535\alpha a_3 a_4 + 0.125828\alpha a_4^2 - 66.7744a_5 + 0.241626\alpha a_5 \\
&\quad - 1.50887\alpha a_1 a_5 + 2.86511\alpha a_2 a_5 - 0.415733\alpha a_3 a_5 + 0.272801\alpha a_4 a_5 + 4.4739\alpha a_5^2 \\
&\quad - 1.5a_2^3, \\
\dot{a}_3 &= -72.8953a_1 + 0.725986\alpha a_1 + 0.05655\alpha a_1^2 + 122.542a_2 - 1.00856\alpha a_2 \\
&\quad - 3.7576\alpha a_1 a_2 - 5.38241\alpha a_2^2 - 974.508a_3 + 13.4944\alpha a_3 + 0.96696\alpha a_1 a_3 \\
&\quad + 1.19751\alpha a_2 a_3 - 1.3391\alpha a_3^2 - 417.409a_4 + 4.13014\alpha a_4 + 1.63645\alpha a_1 a_4 \\
&\quad + 0.0339751\alpha a_2 a_4 + 0.346602\alpha a_3 a_4 - 1.82304\alpha a_4^2 - 114.944a_5 + 0.220561\alpha a_5 \\
&\quad + 1.56055\alpha a_1 a_5 + 0.424728\alpha a_2 a_5 + 1.44077\alpha a_3 a_5 - 2.93726\alpha a_4 a_5 + 2.98004\alpha a_5^2 \\
&\quad - 1.5a_3^3, \\
\dot{a}_4 &= -12.4719a_1 + 0.375998\alpha a_1 - 0.0939612\alpha a_1^2 - 201.511a_2 + 1.49775\alpha a_2 \\
&\quad - 1.19105\alpha a_1 a_2 + 2.50634\alpha a_2^2 - 417.409a_3 + 4.13014\alpha a_3 - 2.23219\alpha a_1 a_3 \\
&\quad - 2.99006\alpha a_2 a_3 - 2.65047\alpha a_3^2 - 606.794a_4 + 6.63728\alpha a_4 - 0.127752\alpha a_1 a_4 \\
&\quad - 4.22894\alpha a_2 a_4 - 2.46861\alpha a_3 a_4 - 1.20316\alpha a_4^2 - 431.498a_5 + 3.58672\alpha a_5 \\
&\quad - 1.29591\alpha a_1 a_5 - 3.05007\alpha a_2 a_5 + 1.24718\alpha a_3 a_5 - 1.27468\alpha a_4 a_5 - 2.0206\alpha a_5^2 \\
&\quad - 1.5a_4^3, \\
\dot{a}_5 &= 34.6688a_1 - 0.561543\alpha a_1 + 0.0642473\alpha a_1^2 - 66.7744a_2 + 0.241626\alpha a_2 \\
&\quad + 0.619004\alpha a_1 a_2 - 0.548517\alpha a_2^2 - 114.944a_3 + 0.220561\alpha a_3 - 2.09107\alpha a_1 a_3 \\
&\quad + 0.162558\alpha a_2 a_3 + 0.44833\alpha a_3^2 - 431.498a_4 + 3.58672\alpha a_4 + 0.701577\alpha a_1 a_4 \\
&\quad + 1.57101\alpha a_2 a_4 + 1.43951\alpha a_3 a_4 + 0.0387317\alpha a_4^2 - 1285.02a_5 + 14.8582\alpha a_5 \\
&\quad - 0.0898619\alpha a_1 a_5 - 1.60065\alpha a_2 a_5 - 2.34221\alpha a_3 a_5 - 1.37323\alpha a_4 a_5 + 1.09346\alpha a_5^2 \\
&\quad - 1.5a_5^3.
\end{aligned}
\tag{A.1}
$$

References

[1] D. Armbruster, J. Guckenheimer, and P. Holmes, *Kuramoto-Sivashinsky dynamics on the center-unstable manifold*, SIAM J. Appl. Math. **49** (1989), no. 3, 676–691.

[2] D. Armbruster, R. Heiland, and E. J. Kostelich, *KLTOOL: a tool to analyze spatiotemporal complexity*, Chaos **4** (1994), no. 2, 421–424.

[3] A. V. Babin and M. I. Vishik, *Attractors of evolution partial differential equations and estimates of their dimension*, Russian Math. Surveys **38** (1983), 151–213.

[4] P. Baldi and K. Hornik, *Neural networks and principal component analysis: learning from examples without local minima*, Neural Netw. **2** (1989), no. 1, 53–58.

[5] H. Bourlard and C. J. Wellekens, *Speech dynamics and recurrent neural networks*, Proc. International Conference on Acoustics, Speech, and Signal Processing. Vol. 1 (Glasgow, UK), 1989, pp. 33–36.

[6] C. Canuto, M. Y. Hussaini, A. Quarteroni, and T. A. Zang, *Spectral Methods in Fluid Dynamics*, Springer Series in Computational Physics, Springer-Verlag, New York, 1988.

[7] P. Constantin, C. Foias, B. Nicolaenko, and R. Temam, *Integral Manifolds and Inertial Manifolds for Dissipative Partial Differential Equations*, Applied Mathematical Sciences, vol. 70, Springer-Verlag, New York, 1989.

[8] P. Constantin, C. Foias, and R. Temam, *On the dimension of the attractors in two-dimensional turbulence*, Phys. D **30** (1988), no. 3, 284–296.

[9] C. Foias, G. R. Sell, and R. Temam, *Inertial manifolds for nonlinear evolutionary equations*, J. Differential Equations **73** (1988), no. 2, 309–353.

[10] C. Foias and R. Temam, *On the Hausdorff dimension of an attractor for the two-dimensional Navier-Stokes equations*, Phys. Lett. A **93** (1983), no. 9, 451–454.

[11] R. Gonzalez-Garcia, R. Rico-Martinez, W. Wolf, M. Lübke, M. Eiswirth, J. S. Anderson, and I. G. Kevrekidis, *Characterization of a two-parameter mixed-mode electrochemical behavior regime using neural networks*, Phys. D **151** (2001), no. 1, 27–43.

[12] H. Harman, *Modern Factor Analysis*, The University of Chicago Press, Illinois, 1960.

[13] D. Henry, *Geometric Theory of Semilinear Parabolic Equations*, Lecture Notes in Mathematics, vol. 840, Springer-Verlag, New York, 1981.

[14] H. Hotelling, *Analysis of a complex of statistical variables into principal components*, J. Educ. Psychol. **24** (1933), 417–441; 498–520.

[15] J. M. Hyman, B. Nicolaenko, and S. Zaleski, *Order and complexity in the Kuramoto-Sivashinsky model of weakly turbulent interfaces*, Phys. D **23** (1986), no. 1–3, 265–292.

[16] I. T. Jolliffe, *Principal Component Analysis*, Springer Series in Statistics, Springer-Verlag, New York, 1986.

[17] I. G. Kevrekidis, B. Nicolaenko, and C. Scovel, *Back in the saddle again: a computer assisted study of the Kuramoto-Sivashinsky equation*, SIAM J. Appl. Math. **50** (1990), no. 3, 760–790.

[18] M. Kirby and D. Armbruster, *Reconstructing phase space from PDE simulations*, Z. angew. Math. Phys. **43** (1992), no. 6, 999–1022.

[19] M. A. Kramer, *Nonlinear principal component analysis using autoassociative neural networks*, AIChE J. **37** (1991), no. 2, 233–243.

[20] Y. Kuramoto and T. Tsuzuki, *Persistent propagation of concentration waves in dissipative media far from thermal equilibrium*, Progr. Theoret. Phys. **55** (1976), 356–369.

[21] O. A. Ladyzhenskaya, *Finite-dimensionality of bounded invariant sets for Navier-Stokes systems and other dissipative systems*, J. Soviet Math. **28** (1985), 714–726.

[22] E. N. Lorenz, *Deterministic nonperiodic flow*, J. Atmospheric Sci. **20** (1963), 130–141.

[23] J. L. Lumley, *The structure of inhomogeneous turbulent flows*, Atmospheric Turbulence and Radio Wave Propagation (A. M. Yaglom and V. I. Tatarski, eds.), Nauka, Moscow, 1967, pp. 166–178.

[24] J. Mallet-Paret, *Negatively invariant sets of compact maps and an extension of a theorem of Cartwright*, J. Differential Equations **22** (1976), no. 2, 331–348.
[25] R. Mañé, *On the dimension of the compact invariant sets of certain nonlinear maps*, Dynamical Systems and Turbulence, Warwick 1980 (Coventry, 1979/1980), Lecture Notes in Math., vol. 898, Springer, Berlin, 1981, pp. 230–242.
[26] D. W. Marquardt, *An algorithm for least-squares estimation of nonlinear parameters*, J. Soc. Indust. Appl. Math. **11** (1963), 431–441.
[27] R. Martinez, R. K. Krischer, I. G. Kevrekidis, M. Kube, and J. L. Hudson, *Discrete- vs. continuous-time nonlinear signal processing of Cu electrodissolution data*, Chem. Eng. Comm. **118** (1992), 25–48.
[28] L. Sirovich, *Turbulence and the dynamics of coherent structures. I. Coherent structures*, Quart. Appl. Math. **45** (1987), no. 3, 561–571.
[29] N. Smaoui, *Artificial neural network-based low-dimensional model for spatio-temporally varying cellular flames*, Appl. Math. Modelling **21** (1997), 739–748.
[30] _____, *An artificial neural network noise reduction method for chaotic attractors*, Int. J. Comput. Math. **73** (2000), no. 4, 417–431.
[31] _____, *A model for the unstable manifold of the bursting behavior in the 2D Navier-Stokes flow*, SIAM J. Sci. Comput. **23** (2001), no. 3, 824–839.
[32] _____, *Linear versus nonlinear dimensionality reduction of high-dimensional dynamical system*, SIAM J. Sci. Comput. **25** (2004), no. 6, 2107–2125.
[33] N. Smaoui and S. Al-Yakoob, *Analyzing the dynamics of cellular flames using Karhunen-Loève decomposition and autoassociative neural networks*, SIAM J. Sci. Comput. **24** (2003), no. 5, 1790–1808.
[34] N. Smaoui and D. Armbruster, *Symmetry and the Karhunen-Loève analysis*, SIAM J. Sci. Comput. **18** (1997), no. 5, 1526–1532.
[35] N. Smaoui and M. Zribi, *Controlling the dynamics of the Kuramoto-Sivashinsky equation*, Int. J. Pure Appl. Math. **7** (2003), no. 3, 271–293.

Nejib Smaoui: Department of Mathematics and Computer Science, Kuwait University, P.O. Box 5969, Safat 13060, Kuwait
E-mail address: smaoui@mcs.sci.kuniv.edu.kw